Comparing methods for coupling wake models to an atmospheric perturbation model in WAYVE

Devesse, Koen; Stipa, Sebastiano; Brinkerhoff, Joshua; Allaerts, Dries; Meyers, Johan

DOI
10.1088/1742-6596/2767/9/092079

Publication date
2024

Document Version
Final published version

Published in
Journal of Physics: Conference Series

Comparing methods for coupling wake models to an atmospheric perturbation model in WAYVE

Journal of Physics: Conference Series **2767** (2024) 092079 doi:10.1088/1742-6596/2767/9/092079

Comparing methods for coupling wake models to an atmospheric perturbation model in WAYVE

Koen Devesse[1], Sebastiano Stipa[2], Joshua Brinkerhoff[2], Dries Allaerts[3], Johan Meyers[1]

[1] Department of Mechanical Engineering, KU Leuven, Leuven, Belgium
[2] School of Engineering, University of British Columbia—Okanagan, Kelowna, Canada
[3] Faculty of Aerospace Engineering, Delft University of Technology, Delft, The Netherlands

E-mail: koen.devesse@kuleuven.be

Abstract. As offshore wind farms grow in size, the blockage effect associated with the atmospheric gravity waves they trigger is expected to become more important. To model this, recent research has produced an Atmospheric Perturbation Model (APM), which simulates the mesoscale flow in the atmospheric boundary layer at a low computational cost compared to traditional methods. However, as a simplified reduced-order model, it can not resolve individual turbine wakes, and has to be coupled to an engineering wake model to predict farm power output. Over the years, three coupling methods have been developed, and been combined into the open-source framework WAYVE. This paper compares them, discussing both their theoretical validity and their performance. For the latter, we validate the velocities and power outputs predicted by WAYVE against 27 LES simulations. We find that the velocity matching (VM) and the pressure-based (PB) methods perform the best. Of these two, the VM method is more consistent with the APM output, while the PB method has a significantly lower computational cost.

1. Introduction

Recent research pointed out that the interaction of large offshore turbine clusters with the stratified atmospheric boundary layer (ABL) can greatly impact the power yield of wind farms ([1, 2, 3], among others). Specifically, the vertical perturbation of the incoming flow by the wind farm triggers gravity waves in the thermally stratified free atmosphere, producing pressure perturbations that are felt inside the boundary layer. These perturbations in pressure alter the mean flow impinging the wind turbines, ultimately reducing or increasing their produced power. The importance of such dynamics, which increase with the size of the wind farm, is currently misrepresented or disregarded by conventional engineering models, whereas high-fidelity computational fluid dynamics (CFD) tools are too expensive to be used for wind-farm planning and annual energy predictions. To address this, Allaerts and Meyers [4] developed an Atmospheric Perturbation Model (APM) that predicts the atmospheric response to an horizontally Gaussian-filtered wind farm thrust distribution. While being orders of magnitude faster than large eddy simulations (LESs) or numerical weather models such as the Weather Research & Forecasting (WRF) model, the APM only focuses on the mesoscale physics and its resolution is too coarse to resolve individual wind turbine wakes. As a consequence, the APM needs to be coupled with an engineering wake model in order to capture turbine–turbine interactions. To achieve this, three different approaches have been developed so far, namely the

Upstream (US) coupling method originally developed by Allaerts and Meyers [4], the *Velocity Matching* (VM) technique [5], and the *Pressure-Based* (PB) velocity reconstruction [6]. All three coupling methods have been implemented in a new open-source code, called WAYVE (Wind-fArm gravitY-waVe and blockagE), which will be used in this paper [7].

In the current work, we will validate the different coupling strategies using 27 LES simulations from a database produced by Lanzilao and Meyers [3], comparing them against each other in order to asses their performance with varying free atmosphere stability and boundary layer height. Additionally, we discuss their computational cost, potential complications in using them with other codes, and whether the turbine-level velocity fields satisfy the governing equations of the APM, which we refer to as the *consistency* of the coupling method.

The remainder of this paper is structured as follows. Section 2 gives an overview of the APM, the wake model, and the three coupling methods. Section 3 compares the results obtained with WAYVE to the LES data from Lanzilao and Meyers [3]. Finally, section 4 draws some conclusions and gives recommendations for future work.

2. Methodology

This section gives an overview of the APM, the wake model, and the coupling strategies analyzed in this paper. Moreover, we discuss the consistency of the coupling methods, defined as the ability of the velocity fields predicted by the coupled wake model to satisfy the governing equations of the APM.

2.1. Atmospheric Perturbation Model

The APM simulates the ABL as two vertically homogeneous layers of fluid, topped by a capping inversion characterized by a potential temperature jump $\Delta\theta$ and a stratified free atmosphere with a lapse rate Γ. This replicates the typical vertical structure of conventionally neutral boundary layers (CNBLs) found offshore. The APM is derived by applying two operations to the Reynolds-averaged continuity and momentum equations for steady-state, incompressible flow. First, the equations are filtered by means of an horizontal Gaussian filter with a filter length of 1 km, in order to reduce the model to a mesoscale resolution. Secondly, the equations are height-averaged in each of the two layers. A thorough derivation of the APM can be found in Devesse et al. [5]. The resulting model structure is shown schematically in figure 2 of Allaerts and Meyers [4].

The resulting APM consists of two sets of depth-averaged linearized continuity and momentum equations in each layer, namely

$$U_{j,1}\frac{\partial u'_{i,1}}{\partial x_j} = -\frac{1}{\rho_0}\frac{\partial p}{\partial x_i} + f_c\epsilon_{ij3}u'_{j,1} + \nu_{t,1}\frac{\partial^2 u'_{i,1}}{\partial x_j \partial x_j} + \frac{D_{ij}}{H_1}\Delta_1^2 u'_j - \frac{C_{ij}}{H_1}u'_{j,1} - \frac{T_{i3,1}-T_{i3,0}}{H_1^2}\eta_1 + (F_i + \Delta\tau_{wf,i})\left(\frac{1}{H_1} - \frac{\eta_1}{H_1^2}\right) - \frac{\partial \tau_{d,ij}}{\partial x_j}, \tag{1}$$

$$U_{j,2}\frac{\partial u'_{i,2}}{\partial x_j} = -\frac{1}{\rho_0}\frac{\partial p}{\partial x_i} + f_c\epsilon_{ij3}u'_{j,2} + \nu_{t,2}\frac{\partial^2 u'_{i,2}}{\partial x_j \partial x_j} - \frac{D_{ij}}{H_1}\Delta_1^2 u'_j + \frac{T_{i3,1}}{H_2^2}\eta_2 - \Delta\tau_{wf,i}\left(\frac{1}{H_2} - \frac{\eta_2}{H_2^2}\right), \tag{2}$$

$$U_{j,1}\frac{\partial \eta_1}{\partial x_j} + H_1\frac{\partial u'_{j,1}}{\partial x_j} = 0, \tag{3}$$

$$U_{j,2}\frac{\partial \eta_2}{\partial x_j} + H_2\frac{\partial u'_{j,2}}{\partial x_j} = 0, \tag{4}$$

where $u'_{i,1}$, $u'_{i,2}$, η_1, and η_2 (with $i = 1, 2$) are the perturbations to the unperturbed depth-averaged wind speeds $U_{i,1}$ and $U_{i,2}$ and the layer heights H_1 and H_2. The subscripts 1 and 2

denote the lower and upper layer, respectively. The first five terms of equations 1 and 2 represent the advection of momentum, the pressure gradients induced by gravity waves, the Coriolis forces, the horizontal turbulent momentum fluxes, and the turbulent momentum exchange between the layers due to the velocity difference between them. The C_{ij} term in equation 1 represents the momentum exchange with the ground. Next, the terms scaling with η_1 and η_2 give the effect of the background momentum fluxes $T_{i3}(z)$ being distributed over thinner or thicker layers of fluid. All of the terms mentioned so far are linear with respect to the APM state.

The remaining terms in equations 1 and 2 are the direct effects of the wind farm. The turbine forces F_i are only felt in the lower layer, while the increased entrainment of momentum above the farm $\Delta\tau_{wf,i}$ is present in both layers. The turbine forces are computed by coupling to an engineering wake model, as explained in the following sections. Finally, $\tau_{d,ij}$ are the dispersive stresses due to sub-grid flow heterogeneity, which appear when applying the horizontal filtering operator:

$$\tau_{d,ij} = \frac{1}{H_1 + \eta_1} \int_0^{H_1+\eta_1} \mathcal{G}\left(\left(u_{w,i} - \mathcal{G}\left(u_{w,i}\right)\right)\left(u_{w,j} - \mathcal{G}\left(u_{w,j}\right)\right)\right) \mathrm{d}z, \tag{5}$$

where u_w are the turbine-level velocities, and $\mathcal{G}$ is the horizontal Gaussian filter. Like the turbine forces, these velocities u_w are found using an engineering wake model. This constitutes the main computational cost of the APM, as the turbine-level velocities have to be evaluated on a relatively fine grid. Furthermore, this parametrization underestimates the dispersive stresses by 30-50%, and is one of the main sources of error at the farm entrance. For an in-depth discussion of the wind farm representation, see Devesse et al. [5].

Within the ABL, the flow is assumed to be hydrostatic, so the pressure perturbation is taken at the top of the ABL. Here, the pressure can be related to the effect of two types of gravity waves, which form due to the displacement of the capping inversion $\eta_t = \eta_1 + \eta_2$. The first of these two types are referred to as interfacial waves, which correspond directly to the inversion layer displacement. Their pressure feedback $p_{\text{interfacial}}$ scales with the reduced gravity $g' = g\Delta\theta/\theta$ [8] as

$$\frac{p_{\text{interfacial}}}{\rho_0} = g'\eta_t. \tag{6}$$

The second type of waves are referred to as internal waves, and are generated as the free atmosphere perceives the displacement of the capping inversion similarly to large-scale topographies as it flows over them [8]. Their pressure feedback p_{internal} can be expressed in Fourier components where, for each wavenumber k and l in the streamwise and spanwise direction, respectively, the pressure scales with the stratification coefficients Φ [8] as

$$\frac{p_{\text{internal}}}{\rho_0} = \mathcal{F}^{-1}\left(\Phi\right) * \eta_t, \qquad \Phi = \frac{\mathrm{i}\left(N_g^2 - \Omega^2\right)}{m}, \tag{7}$$

where $N_g = \sqrt{g\Gamma/\theta}$ is the Brunt-Väisälä frequency, and $\Omega = -U_{g,i}k_i$ is the intrinsic frequency of the waves. The vertical wavenumber m is given by the dispersion relation [9]. The total pressure perturbation in the ABL is obtained by adding the two contributions $p_{\text{interfacial}}$ and p_{internal}.

The APM is solved using a fixed-point iteration with a relaxation factor of 0.7 at a grid resolution of 500 m. At each step, the wind farm effects are computed using the engineering wake model. We use a Fourier-Galerkin spectral method to solve the remaining linear system, as this makes it easy to incorporate the pressure closure equation [4]. Since the matrix decouples per wavenumber, it is computationally cheap to solve [5].

2.2. Wake model

In the present study, we use the wake merging method of Lanzilao and Meyers [10], which allows for heterogeneous background flows. For simplicity, this paper neglects multi-directional

effects and takes the velocity to be in the direction of the unperturbed flow at the hub height. Throughout the remainder of the paper, all velocities will refer to the velocity components in this direction, denoted by x, unless stated otherwise. However, we emphasize that this is not an inherent limitation of the APM, the wake model, or the coupling methods discussed here. For a given background velocity U_b, the wake model velocity field u_w can be calculated as [10]

$$u_w(x,y,z) = U_b(x,y,z) \prod_{k=1}^{N_t} \left[1 - W_k(x,y,z)\right], \tag{8}$$

where N_t is the number of turbines and W_k is the wake deficit function, evaluated using the Gaussian wake model of Bastankhah and Porté-Agel [11]. The evolution of the turbulence intensity, required to compute the wake expansion in the Bastankhah and Porté-Agel model, is incorporated using the model of Niayifar and Porté-Agel [12]. Wind turbines are mirrored to account for ground effects. The wake model is not tuned, and uses the parameters reported in the above papers, as these have been found to perform well for neutral flow conditions [5]. Additionally, we use the induction zone model by Troldborg and Meyer Forsting [13] when evaluating the velocity field, but this is not used when calculating the inflow velocities. A more detailed overview of the wake model used in this paper can be found in Devesse et al. [5].

To incorporate the mesoscale effects predicted by the APM, the background velocity U_b in equation 8 has to be based on the APM state. Since the APM output is a perturbation to a background state, and does not vary within a layer, we split up this U_b as:

$$U_b(x,y,z) = U_0(z) + u_b(x,y) f(z), \qquad f(z) = \frac{1}{\kappa} \log\left(\frac{z}{z_0}\right), \tag{9}$$

where U_0 is the unperturbed velocity profile, and f is a standard logarithmic shape function. The goal of the coupling methods described below is to compute u_b based on the APM state.

2.3. Upstream coupling

In their original paper, Allaerts and Meyers [4] use the depth-averaged velocity predicted by the APM at the location ten turbine diameters upstream of the farm entrance as a new uniform background velocity for the wake model. While they directly took U_b to be the APM velocity at that point, we will reconstruct the vertical profile as discussed above:

$$u_b = u_1'(x_u, y_u) \left[\frac{1}{H_1 + \eta_1(x_u, y_u)} \int_0^{H_1 + \eta_1(x_u, y_u)} f \mathrm{d}z \right]^{-1}, \tag{10}$$

where (x_u, y_u) is the location $10D$ upstream of the front turbine.

This ad-hoc approach results in a wake model velocity field that is not guaranteed to be consistent with the APM output. Any mesoscale effects taking place downstream of the farm entrance—e.g. favorable pressure gradients or increased momentum entrainment—are not accounted for. However, it has a negligible computational cost, and does not impose any constraints on the wake model it couples to.

2.4. Velocity matching

Devesse et al. [5] developed a coupling technique based on ensuring that the wake model velocity is consistent with the APM state. Specifically, when the Gaussian filtering and height-averaging operators used in the derivation of the APM are applied to the wake model velocity, it should

match the APM velocity. For a given APM state, the background velocity can be found directly by solving a least-squares problem corresponding to the matching condition

$$\frac{1}{H_1+\eta_1}\int_0^{H_1+\eta_1}\int_{-\infty}^{\infty}\int_{-\infty}^{\infty} G(x-x',y-y') \\ \big(U_0(z)+u_b(x',y')\big)\prod_{k=1}^{N_t}\big[1-W_k(x',y',z)\big]\,\mathrm{d}x'\mathrm{d}y'\mathrm{d}z = U_1+u_1'(x,y), \quad (11)$$

where G is a Gaussian kernel with a filter length of twice the APM grid spacing. It's clear that the resulting velocity field will be fully consistent with the governing equations of the APM.

This approach comes with some drawbacks. First, it requires the initial calculation of the wake deficit shape functions W_k on a relatively fine grid, although this cost is shared with the calculation of the dispersive stresses in their current parametrization. Additionally, equation 11 has to be solved at every step of the fixed-point iteration. Since η_1 changes between steps, the associated matrix can not be precomputed. Finally, the matching condition is closely tied to the wake merging method. The least-squares formulation developed by Devesse et al. requires the wake model to be *self-similar*, i.e. for wakes to be applied through multiplication instead of addition, and has to be modified for other wake merging methods.

2.5. Pressure-based

Stipa et al. [6] integrated the APM into a Multi-Scale Coupled framework, in which it was combined with a wake model and an induction model. The coupling was based on the pressure field generated by the APM. After an initial calculation to obtain the APM state, the model is re-run using the pressure field to force the depth-averaged momentum equation instead of the wind farm forcing terms:

$$U_{j,1}\frac{\partial u_{p,i,1}'}{\partial x_j} = -\frac{1}{\rho_0}\frac{\partial p}{\partial x_i} + A(u_p',\eta_1), \quad (12)$$

where $u_{p,i}'$ is the pressure-driven velocity perturbation. For the sake of brevity, we only show the lower layer momentum equation (eq. 1) and use a simplified notation, where A is a linear operator representing the Coriolis forces, the eddy viscosity term, and the momentum exchange with the ground and between the layers.

The resulting depth-averaged velocity field u_p' is then reconstructed by matching the integral of a logarithmic profile, and used as the background velocity for the wake model, namely

$$u_b = u_{p,1}'\left[\frac{1}{H_1+\eta_1}\int_0^{H_1+\eta_1} f\,\mathrm{d}z\right]^{-1}. \quad (13)$$

The intuition behind this method is to isolate the blockage effect produced by the gravity waves in a separate velocity field, and take the latter as the background flow. There is good indirect evidence to support this, as Devesse et al. [5] found u_b to strongly correlate with the pressure perturbation.

To further analyze the consistency of this approach, we try in the following to provide a theoretical justification. In essence, equation 12 implies a splitting of the APM velocities u_i' into the pressure component $u_{p,i}'$ and a forcing component $u_{f,i}'$. This corresponds to splitting up the governing equations of the APM, so that an equation for $u_{f,i}'$ can be found by subtracting equation 12 from the lower layer momentum equation 1:

$$U_{j,1}\frac{\partial u_{f,i,1}'}{\partial x_j} = (F_i+\Delta\tau_{wf,i})\left(\frac{1}{H_1}-\frac{\eta_1}{H_1^2}\right) - \frac{\partial \tau_{d,ij}}{\partial x_j} + A(u_f',0). \quad (14)$$

So far, the above equations are fully equivalent to the APM, and no approximation has been made. While $u'_{p,i}$ and $u'_{f,i}$ do not satisfy the continuity equations on their own, their sum still does.

Instead of solving for both $u'_{p,i}$ and $u'_{f,i}$, Stipa et al. [6] only solve eq. 12, and apply the wake model to the resulting u_b. Consistency-wise, this implies that the mesoscale effect of applying the wake model to u'_p roughly corresponds to adding u'_f:

$$u'_{p,i} + u'_{f,i} \approx \frac{1}{H_1 + \eta_1} \int_0^{H_1+\eta_1} \mathcal{G}\left(u_{w,i}\right) \mathrm{d}z, \tag{15}$$

where u_w is based on $u'_{p,i}$ through equation 13.

This requires the wake model to accurately capture the mesoscale effects of the turbine forces, increased turbulent entrainment above the farm, and the dispersive stresses. In essence, this is approximately what wake models are designed to do: predicting turbine-level velocity fields in the absence of large-scale velocity or pressure gradients, which corresponds to neutral flow. Devesse et al. [5] indeed found that the mesoscale velocity deficit of the wake model used here is very similar to that found by LES in neutral conditions. The main difference between equation 14 and the APM equations for neutral flow, is that the former does not include the hydrodynamic pressure perturbations in the free atmosphere.

While the coupling does require 2 additional momentum equations to be solved at each step, it is still relatively computationally cheap as the system of equations decouples per wavenumber. Furthermore, like the US method, it is independent of the formulation of the underlying wake model, which makes it easy to interface to other wake model codes.

3. Results

In this secton, we compare results obtained from each of the coupling methods to the LES data from Lanzilao and Meyers [3]. These are all simulations of the same large wind farm of $N_t = 160$ IEA 10 MW turbines, arranged in a staggered layout with 16 rows and 10 columns. The dataset is parametric in the boundary layer heights H, capping inversion strengths $\Delta\theta$ and free atmosphere stratification Γ. From the original dataset of 40 cases, we leave out the fully neutral cases and those with a boundary layer height of 150 m, as the current formulation of the APM is not yet suited for simulating these conditions. This leaves 27 cases, with a parameter scope of $H = 300, 500, 1000$ m, $\Delta\theta = 2, 5, 8$ K, and $\Gamma = 1, 4, 8$ K/km. A detailed description of the LES setup and wind-farm characteristics can be found in Lanzilao and Meyers [3].

3.1. Velocity fields

We now discuss the velocity fields predicted by the APM with the different coupling methods, and compare them to the LES results. To do this, we construct APM states from the LES data by applying the horizontal filtering and height-averaging operations. This allows to make direct comparisons with the mesoscale APM velocities. For a detailed description of this procedure, we refer to Devesse et al. [5].

Following Devesse et al. [5], we will focus on the case H1000-$\Delta\theta$5-Γ1, which is the case where $H = 1000$ m, $\Delta\theta = 5$ K, and $\Gamma = 1$ K/km, as it is representative of the overall dataset. In particular, it features blockage effects and resonant lee waves throughout the farm. Figure 1 shows the mesoscale velocity perturbation (u'_1) in the lower layer for the LES-based state and the APM. While the different coupling methods result in slight changes in the APM states, there are no large qualitative differences between them. The APM underestimates the velocity deficit at the farm entrance, but overestimates it in the second half of the farm, a trend which holds for almost all of the analyzed cases. A full discussion of the APM performance can be found in Devesse et al. [5].

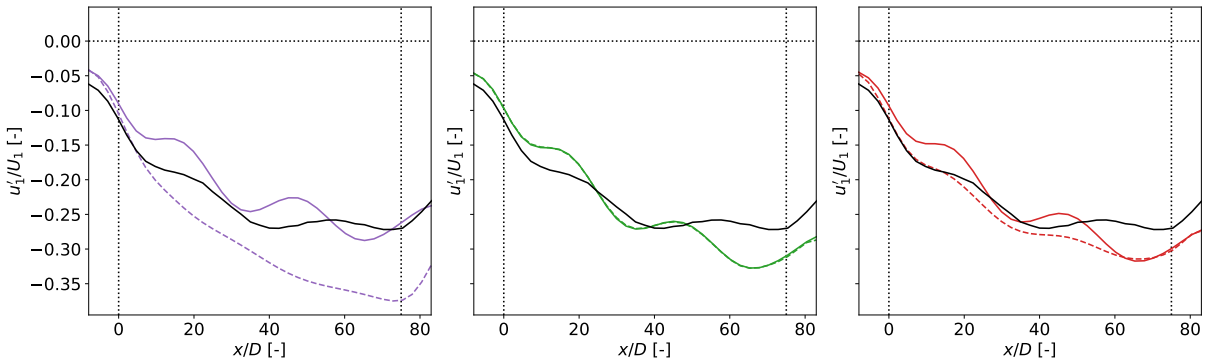

Figure 1. Mesoscale velocity fields for the case H1000-$\Delta\theta$5-Γ1 as found by LES (full lines, black), and the APM, using the US (purple, left), VM (green, middle), and PB (red, right) coupling methods. The dashed lines show the reconstructed mesoscale velocity, based on the wake model velocity predictions. The dotted lines denote the wind farm region.

While the choice of coupling method does not significantly impact the direct APM state, it has a large effect on the velocity fields produced by the wake model. We will discuss this on a mesoscale level, to show how consistent the results are with the APM state. Figure 1 also shows the reconstructed mesoscale velocities for the different coupling methods, which were obtained by horizontally filtering and height-averaging the wake model velocity fields u_w. The US method results in a wake model velocity with a constant background. This leads to a severe underestimation of the velocity throughout the farm, as the favorable effect of the pressure gradient behind the farm entrance is not taken into account. It is also clear that the resulting velocity field is not consistent with the continuity or momentum equations of the APM. In contrast, the VM method reproduces the APM state almost exactly, by construction. Finally, while the PB method does deviate significantly from the APM, it does capture the general trends, with both the resonant lee waves and the velocity recovery at the end of the farm being clearly visible.

As noted above, the APM underestimates the velocity deficit at the farm entrance. This is primarily due to an underestimation of the dispersive stresses, which play an important role in this region [5]. The VM method reproduces this, as it pushes u_w towards the APM velocity. In contrast, the PB method results in an accurate reproduction of the mesoscale state at the farm entrance. We hypothesize that this is because the pressure perturbation is less affected by the accuracy of the wind farm parametrization than the velocity. Since the PB method uses the pressure to calculate u_b, it would then also be less dependent on these parametrizations.

3.2. Power output

Following Allaerts and Meyers [1], we define the farm (η_f), non-local (η_{nl}), and wake (η_w) efficiencies as

$$\eta_f = \eta_{nl}\eta_w, \quad \eta_{nl} = \frac{P_1}{P_0}, \quad \eta_w = \frac{P_{avg}}{P_1}, \tag{16}$$

where P_0, P_1, and P_{avg} are the power outputs of a free-standing turbine, a front-row turbine, and the average turbine across the farm [1, 3]. The non-local efficiency η_{nl} is a measure for the effect of blockage on front row performance, while the wake efficiency η_w measures the favourable effects of the downstream pressure gradients and increased momentum flux.

Figure 2 shows the efficiencies from all 27 analyzed cases for the three coupling methods, compared to the LES results. The average values across all cases are shown in table 1. A standalone wake model case without APM coupling is also included for reference. It's

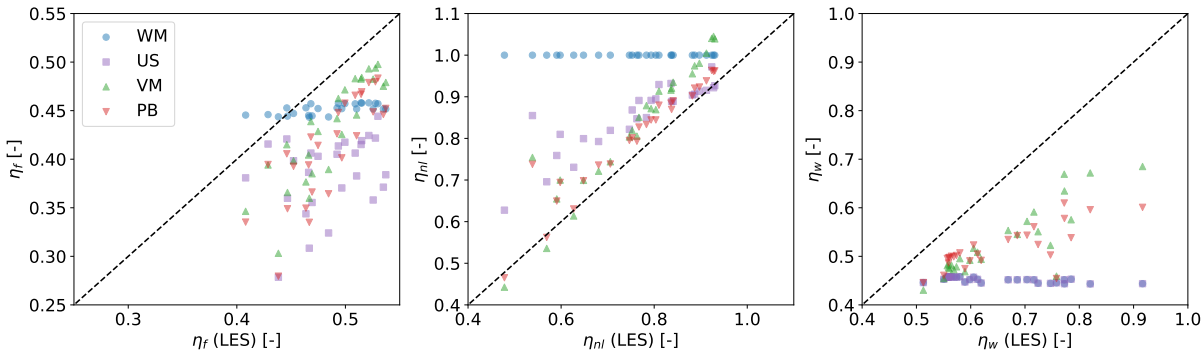

Figure 2. Farm (left), non-local (middle), and wake (right) efficiencies for uncoupled wake model (blue, ○) and the APM with the US (purple, □), VM (green, △), and PB (red, ▽) coupling methods, as compared to LES.

Table 1. Average farm, non-local, and wake efficiencies as predicted by the different methods across all cases.

Method	η_f [%]	η_{nl} [%]	η_w [%]
LES	48.6	76.0	65.5
Uncoupled wake model	45.1	100.0	45.1
Upstream (US)	38.6	85.4	45.1
Velocity Matching (VM)	43.0	83.3	52.7
Pressure-based (PB)	41.3	80.5	51.8

clear that blockage effects are large, as η_{nl} varies between 0.55 and 1. All coupling methods significantly outperform the standard wake model, as the latter does not predict any upstream wind deceleration.

The US method gives good results when predicting η_{nl}, and could probably perform better with some tuning of the distance at which u_b is evaluated. However, due to the ad-hoc nature of the method, this might not hold for other farm layouts. Furthermore, since it only includes information upstream of the farm, it predicts the same η_w as the uncoupled wake model. Both the VM and PB methods improve on this, and reproduce some of the variation in η_w as well. While the VM method accurately captures the trend in η_{nl}, it has a consistent overestimation of roughly 5%, leading it to predict $\eta_{nl} > 1$ for four cases where there is very little blockage. This is the result of the VM method reproducing the underestimation of the dispersive stresses at the farm entrance. The PB method avoids this problem, as it does not explicitly depend on the farm parametrization in its coupling, and reproduces the front row power output accurately.

While blockage effects are captured well overall by the different coupling strategies, the wake efficiency shows larger discrepancies. This is caused by two factors. First, the coupling methods over- and underestimate the velocity in the first and second half of the farm, respectively. Second, the background flow provided to the wake model by the coupling methods is only heterogeneous in the wind speed, while a uniform direction is assumed. This results in all turbines being waked, while in reality the mesoscale perturbation in wind direction causes some wake deflection and consequently only partial waking throughout the wind farm [3].

3.3. Computational cost

We now compare the computational cost of running the APM with the different coupling methods. This is complicated by the fact that in the current setup, the computational cost of the APM is dominated by the parametrization of the dispersive stresses, which requires the initial computation of u_w, or equivalently W_k, on a relatively fine grid. The VM method also needs this calculation for its matching condition, while the US and PB methods do not. This makes the total runtime of the APM with different coupling methods an incomplete metric of their cost.

Therefore, we split up the computational cost into components related to the APM, the dispersive stresses, and the coupling methods. The APM components are the costs associated with solving the governing equations (eqs. 1-4) and setting up the various parametrizations, except those for the dispersive stresses, which form their own component. The coupling components are the costs associated with calculating the turbine inflow velocities, including running the wake model itself. Moreover, we divide these components further into the preprocessing costs, which have to be done once, and repeated costs, which have to be repeated at every step of the fixed point iteration.

Table 2 shows the results, normalized by the cost of a single wake model run. The cost of compiling the wake model has been left out. It's clear that the VM method is by far the most expensive, roughly doubling the total computational cost per iteration of the APM. In contrast, the US and PB methods have computational costs comparable to the underlying wake model, which makes the APM and dispersive stress components the computational bottleneck. The high cost of the VM method is due to two factors. First, the calculation of W_k and solving the least-squares problem result in inherently high pre-processing and repeated costs, respectively. Secondly, much of the implementation of the VM method in WAYVE is done in native Python, which might change with future development.

Table 2. Computing times of the different components, normalized by the runtime of a single wake model run. The asterisks denote a shared cost.

Component	Pre-processing [-]	Repeated [-]
APM	50	250
Dispersive stresses	800*	230
Upstream (US)	1	1
Velocity Matching (VM)	800*	400
Pressure-based (PB)	70	16

Finally, we want to emphasize that the overall cost of the APM with all three methods is still low compared to conventional CFD tools [14], with the largest total runtime in this work being roughly ten minutes on a standard laptop.

4. Conclusions

The goal of this study was to compare the performance of three different methods of coupling a mesoscale APM to engineering wake models, namely the original upstream (US) method of Allaerts and Meyers [4], the velocity matching (VM) method of Devesse et al. [5], and the pressure-based (PB) method of Stipa et al. [6]. This was done using the open-source WAYVE framework [7], which provides an implementation of both the APM, the unidirectional wake merging method of Lanzilao and Meyers [10], and all three coupling methods. We compared the velocity fields, both at the meso- and microscale, and the farm performance against 27

LES simulations from Lanzilao and Meyers [3]. We also discussed whether the velocity fields produced by the methods are consistent with the governing equations of the APM in terms of how accurately the velocity predicted by the wake model matches with the APM when subjected to the same filtering and height-averaging operations.

All three methods consistently outperform the uncoupled wake model, with the VM and PB method giving the best predictions of the turbine power output. The VM method has the advantage of being the most consistent of the methods analyzed, which allows to best translate the mesoscale APM state to turbine-level velocity fields, albeit at a significant computational cost. However, this results in transferring any issues present in the APM to the wake model. Specifically, this leads to a consistent overestimation of front row power. In contrast, while the PB method is slightly inconsistent in its formulation, it does not have any of the drawbacks of the VM method.

In the current version of the APM, the computational cost of the model is dominated by the dispersive stresses. While the VM method requires these calculations for its matching conditions as well, the US and PB methods do not. A cheaper and more accurate parametrization of these terms would reduce the computational cost of the latter by an order of magnitude, while improving the accuracy of the VM method.

Finally, we note that the APM would benefit from more validation campaigns, particularly comparisons against operational data.

Acknowledgments

This research has been supported by the Energy Transition Fund of the Belgian Federal Public Service for Economy, SMEs, and Energy (FOD Economie, K.M.O., Middenstand en Energie), and by the European Union Horizon Europe Framework programme (HORIZON-CL5-2021-D3-03-04) under grant agreement no. 101084205. The computational resources and services in this work were provided by the VSC (Flemish Supercomputer Center), funded by the Research Foundation Flanders (FWO) and the Flemish Government department EWI.

References

[1] Allaerts D and Meyers J 2018 *Boundary-Layer Meteorology* **166** 269–299 ISSN 15731472
[2] Maas O 2023 *Frontiers in Mechanical Engineering* **9** 1–23 ISSN 2297-3079 URL https://www.frontiersin.org/articles/10.3389/fmech.2023.1108180/full
[3] Lanzilao L and Meyers J 2024 *Journal of Fluid Mechanics* **979** A54 ISSN 0022-1120 (*Preprint* 2306.08633) URL http://arxiv.org/abs/2306.08633 https://www.cambridge.org/core/product/identifier/S0022112023010881/type/journal$_a$*rticle*
[4] Allaerts D and Meyers J 2019 *Journal of Fluid Mechanics* **862** 990–1028 ISSN 14697645
[5] Devesse K, Lanzilao L and Meyers J 2023 (*Preprint* 2310.18748) URL http://arxiv.org/abs/2310.18748
[6] Stipa S, Ajay A, Allaerts D and Brinkerhoff J 2023 *Wind Energy Science Discussions (Preprint)* 1–44
[7] Devesse K, Lanzilao L, Allaerts D, Jamaer S and Meyers J 2023 Wind-fArm gravitY-waVe and blockagE code URL https://doi.org/10.48804/XMNVVY
[8] Smith R B 2010 *Wind Energy* **13** 449–458 ISSN 10954244
[9] Gill A E 1982 *Atmosphere-Ocean Dynamics* International geophysics series 30 (San Diego, USA: Academic Press) ISBN 0122835204
[10] Lanzilao L and Meyers J 2022 *Wind Energy* **25** 237–259 ISSN 1095-4244 (*Preprint* 2010.03873) URL https://onlinelibrary.wiley.com/doi/10.1002/we.2669
[11] Bastankhah M and Porté-Agel F 2014 *Renewable Energy* **70** 116–123 ISSN 09601481 URL http://dx.doi.org/10.1016/j.renene.2014.01.002
[12] Niayifar A and Porté-Agel F 2016 *Energies* **9** 741 ISSN 1996-1073 URL http://www.mdpi.com/1996-1073/9/9/741
[13] Troldborg N and Meyer Forsting A R 2017 *Wind Energy* **20** 2011–2020 ISSN 10954244 URL https://onlinelibrary.wiley.com/doi/10.1002/we.2137
[14] van der Laan M P, Sørensen N N, Réthoré P E, Mann J, Kelly M C, Troldborg N, Hansen K S and Murcia J P 2015 *Wind Energy* **18** 2065–2084